The deubiquitinating enzyme inhibitor PR-619 is a potent DNA topoisomerase II poison

Ian G. Cowell, Elise M. Ling, Rebecca L. Swan, Matilda L. W. Brooks, & Caroline A. Austin

Institute for Cell and Molecular Biosciences, Newcastle University, Newcastle upon Tyne. NE2 4HH. U.K. (I.G.C., E.M.L, R.L.S., M.L.W.B,. & C.A.A.)

MOL # 117390

Running title: PR-619 is a TOP2 poison

Corresponding authors

To whom correspondence should be addressed:

Dr Ian G. Cowell and Professor Caroline A. Austin

Institute for Cell and Molecular Biosciences, Newcastle University, Newcastle upon Tyne

NE2 4HH. United Kingdom

Tel: +44 (0)191 208 7677

Fax: +44 (0)191 208 7424

Email: Ian.cowell@ncl.ac.uk

Manuscript information

24 text pages including references and Figure legends

8 figures

0 tables

48 number of references

185 words in abstract

586 words in Introduction

920 words in Discussion

Non standard abbreviations

DMSO, Dimethyl sulfoxide; DSB, DNA double-strand break; DUB, deubiquitinating enzyme inhibitor; H2AX, histone H2A.X; γH2AX, S-139 phospho-histone H2A.X; TOP2A, DNA Topoisomerase IIα; TOP2B, DNA topoisomerase IIβ; TOP2, DNA topoisomerase II.

Abstract

PR-619 (2,6-diaminopyridine-3,5-bis(thiocyanate)) is a broad-spectrum deubiquitinating enzyme (DUB) inhibitor that has been employed in cell-based studies as a tool to investigate the role of ubiquitination in various cellular processes. Here we demonstrate that in addition to its action as a DUB inhibitor, PR-619 is a potent TOP2 poison, inducing both TOP2A and TOP2B covalent DNA complexes with similar efficiency to the archetypal TOP2 poison etoposide. However, in contrast to etoposide which induces TOP2-DNA complexes with a pan-nuclear distribution, PR-619 treatment results in nucleolar concentration of TOP2A and TOP2B. Notably, neither the induction of TOP2-DNA covalent complexes nor their nucleolar concentration are due to TOP2 hyperubiquitination, as both occur even under conditions of depleted ubiquitin. Since like etoposide, PR-619 affected TOP2 enzyme activity in *in vitro* enzyme assays as well as in live cells, we conclude that PR-619 interacts directly with TOP2A and TOP2B. The concentration at which PR-619 exhibits robust cellular DUB inhibitor activity (5-20μM) is similar to the lowest concentration at which TOP2 poison activity was detected (above 20μM), which suggests that caution should be exercised when employing this DUB inhibitor in cell-based studies.

Introduction

Ubiquitination is a post-translational modification where the polypeptide ubiquitin is attached to lysine residues of substrate proteins. This process is reversible, and ubiquitin removal is orchestrated by a large family of deubiquitinating enzymes (DUBs) which fall into six sub-families based on sequence and domain similarity (Harrigan et al., 2018). Five of the sub-families, which contain the majority of the DUBs, are cysteine peptidases. Ubiquitination and deubiquitination together with proteasomal activity control many aspects of cell physiology and many of the enzymes involved have been implicated in human disorders, including cancer. As a result they are an important focus of drug development programs (Huang and Dixit, 2016; Manasanch and Orlowski, 2017; Harrigan et al., 2018). A considerable number of small molecule inhibitors of specific DUBs are now in preclinical development (D'Arcy et al., 2015; Harrigan et al., 2018). These compounds are not only important as potential clinical leads but provide tools to probe the physiological functions of specific DUBs and of ubiquitination in general. While most of the reported small molecule inhibitors exhibit specificity for particular DUBs, PR-619 (2,6-diaminopyridine-3,5-bis(thiocyanate)) is a broad spectrum DUB inhibitor, that nonetheless does not target other cysteine proteases such as cathepsin B or calpain 1 (Altun et al., 2011). In cell-based assays PR-619 was shown to substantially inhibit the activity of USP-, UCH-, OUT- and MJG-class DUBs when applied at 20-50μM, and exhibited a clear effect at a concentration as low as 5μM (Altun et al., 2011). PR-619 has been employed as a tool to investigate the role of ubiquitination in cellular processes including lysosomal degradation (Balut et al., 2011), caspase activation (Crowder et al., 2016), the stability of Sirtuin-7 (Pandey and Kumar, 2015), protein aggregate formation (Seiberlich et al., 2012), HIV replication (Setz et al., 2017) and oocyte maturation (Wang et al., 2017) as well as in the analysis of ubiquitin chain structure (Rana et al., 2017). In addition, PR-619 also inhibited the deSUMOylating enzyme SENP6 in vitro and leads to accumulation of SUMOylated proteins in cells (Altun et al., 2011; Barry et al., 2018)

4

As described above, PR-619 was characterised as a broad-spectrum DUB inhibitor (Altun *et al.*, 2011). We report here that in addition to this activity, PR-619 affects DNA topoisomerase II (TOP2) and causes the accumulation of abundant TOPA and TOP2B covalent DNA complexes in cells, with similar efficiency to the classical TOP2 poison etoposide. TOP2 enzymes alter DNA topology by forming a short-lived enzyme-bridged DNA double-strand break (DSB) where subunits of the dimeric TOP2 enzyme remain covalently attached to each end of the DSB via a 5'-phosphotyrosyl linkage. A second DNA segment then passes through the enzyme-bridged DNA gate, and finally the break is re-ligated by the enzyme, completing the reaction cycle. TOP2 poisons such as etoposide are used in anti-cancer therapies; they inhibit the religation step of the enzyme's reaction cycle, resulting in the persistence of covalently linked TOP2-DNA complexes (Cowell and Austin, 2012) which can be converted to DNA DSBs and are cytotoxic. These covalent complexes can be detected and quantified using the trapped in agarose DNA immunostaining (TARDIS) assay (Willmore *et al.*, 1998; Cowell *et al.*, 2011; Cowell and Austin, 2018). We demonstrate here that PR-619 induces TOP2A and TOP2B covalent DNA complexes and redistribution of TOP2 in the nucleus. Surprisingly, we found that these effects occurred even under conditions of depleted ubiquitin, leading us to conclude that they are independent of the DUB inhibitory activity of PR-619, and thus probably result from direct interaction with TOP2, interfering with its religation activity.

Materials and Methods

Reagents and antibodies. Etoposide and 2-DO8 (2',3',4'-trihydroxy-flavone) were purchased from Sigma-Aldrich (Dorset, UK). PR-619 (2,6-Diamino-3,5-dithiocyanopyridine) was from Tocris Biosciences (Bristol UK), MLN7243 (TAK-243, {(1R,2R,3S,4R)-2,3-Dihydroxy-4-[(2-{3-[(trifluoromethyl)sulfanyl]phenyl}pyrazolo[1,5-a]pyrimidin-7-yl)amino]cyclopentyl}methyl sulfamate was from Active Biochem Ltd (Hong Kong), ML-792 ({{(1R,2S,4R)-4-[(5-{[1-(3-Bromobenzyl)-1H-pyrazol-

3-yl]carbonyl}-4-pyrimidinyl)amino]-2-hydroxycyclopentyl}methyl sulfamate) was from Bioquote (York, UK). Rabbit anti-TOP2A (4566) and anti-TOP2B (4555) antibodies were raised in-house to the C-terminal domains of the respective proteins (Atwal *et al.*, 2019), anti-ubiquitin FK2 (anti-mono and poly-ubiquitinated conjugates, K^{29}, K^{48} or K^{63} linked), catalogue number BML-PW8810 was from Enzo (Exeter, UK). Anti-SUMO2/3 (Ab81371) was from Abcam (Cambridge UK).

Cell Culture. K562 cells were maintained in RPMI-1640 medium supplemented with 10% fetal bovine serum and 1% penicillin and streptomycin (Thermo Fisher Scientific, UK). HeLa cells were cultured in EMEM plus 10% fetal bovine serum and 1% penicillin and streptomycin (Thermo Fisher Scientific, UK). K562 (ATCC CCL-243) and Hela (ECACC 93021013) cell lines were originally sourced from ATCC and ECACC respectively. Cells were cultured at 37°C in a humidified atmosphere containing 5% CO_2. Experiments were conducted on cells growing in log phase. Cells were routinely checked for mycoplasma infection.

Trapped in Agarose DNA Immunostaining (TARDIS) assay. Cells were exposed for 2 hours to etoposide, PR-619 or an equal volume of DMSO and were then pelleted and washed in ice-cold PBS. For TARDIS assays involving HeLa cells, cells were first trypsinised and briefly washed in cold complete cell culture medium. TARDIS assays were carried out essentially as described previously (Willmore *et al.*, 1998; Cowell and Austin, 2018). TOP2 covalent complexes were visualised by immunofluorescence using rabbit anti-TOP2A (4566) or rabbit anti-TOP2B (4555) antibodies raised to the C-terminal domain of human TOP2A and TOP2B respectively and specific mouse antibodies as indicated. Secondary antibodies were AlexaFluor 488 or 594 coupled anti-rabbit or anti-mouse antibodies (Thermo Fisher Scientific, UK). Slides were counterstained with Hoechst 33258 to visualise DNA. Hoechst and AlexaFluor images were captured using an epifluorescence microscope (Olympus IX-81) fitted with an Orca-AG camera (Hamamatsu) and suitable narrow band filter sets. For quantitative analysis images were captured using a 10X objective. After image capture automated slide scoring was performed using Volocity 6.3 software (PerkinElmer Inc.) as described previously (Atwal *et al.*, 2019) using the

same parameters for each slide. Data were subsequently processed and represented using GraphPad

Prism 8.2 (Perkin Elmer, San Diego, CA) and R. For higher resolution qualitative spatial analysis, a 40X

or 60X objective was used and no blinding was applied. Image composites were made with Volocity

6.3 and Adobe Photoshop ensuring that image adjustments were constant between different cell

treatments.

Immunofluorescence analysis using paraformaldehyde fixed samples. K562 cells were washed and

pelleted in ice-cold PBS and spotted onto poly-L-lysine reaction well slides (Marienfeld, VWR

Leicestershire England). Cells were fixed in 4% formaldehyde in PBS at room temperature and

permeabilised using KCM+T buffer (120mM KCl, 20mM NaCl, 10mM Tris-HCl pH 8.0, 1mM EDTA, 0.1%

Triton X-100). After blocking in (KCM+T, 2% Bovine Serum Albumin, 10% dry milk powder) cells were

probed with primary and secondary antibodies as described for TARDIS. Slides were counterstained

with DAPI (Vector Labs, CA) and viewed using an epifluorescence microscope (Olympus IX-81).

Atomated analysis and data presentation were performed as for TARDIS.

DRT analysis. DRT analysis was performed as described previously (Agostinho *et al.*, 2004; I. G. Cowell

et al., 2011). Briefly, HeLa cells were grown on coverslips and were extracted once on ice in DRT buffer

[30 mM HEPES, 65 mM Pipes, 10 mM EGTA, 2 mM MgCl2, pH 6.9 with 350 mM NaCl, 0.5% Triton X-

100] containing protease inhibitors for 30S to 1 min with occasional gentle agitation. Cells were then

fixed with paraformaldehye and imaged as described for immunofluorescence.

In vitro TOP2 assays

Plasmid DNA cleavage reactions were performed as described (Burden *et al.*, 2001). Each reaction

contained 600 ng of purified TOP2A or TOP2B protein and 6.5 μg plasmid DNA TCS1 (Lee *et al.*, 1989).

Precipitated DNA was re-suspended in 15μL of water and 5μL agarose loading buffer (0.5% SDS, 25%

glycerol, 0.1% bromophenol blue). Samples were heated at 70°C for 2 minutes before loading onto a

1% TAE agarose gel and electrophoresed at 45V in 1x TAE. After running, gels were stained with

ethidium bromide and imaged under UV transillumination with Bio-Rad Gel Doc EZ imager. For

7

MOL # 117390

plasmid relaxation assays 10 ng of purified TOP2A or TOP2B protein was incubated at 37°C for 30

minutes with 1.3µg supercoiled plasmid TCS1 in relaxation buffer (50mM Tris pH 7.5, 10mM $MgCl_2$,

0.5mM EDTA, 30µg/mL BSA, 1mM DTT) containing 1mM ATP. Reactions were analysed by

electrophoresis in 0.8% TBE agarose gel. Gels were stained and imaged as above.

Chromatin immunoprecipitation

K562 cells were treated with 80µM PR-619, 100µM etoposide or DMSO (control) for two hours, before

collecting cells by centrifugation and washing twice with ice-cold PBS. Crosslinking was performed

with 1% paraformaldehyde for 5 minutes on ice and paraformaldehyde was quenched with glycine.

Cell pellets were frozen at -80°C. Pellets were thawed in (5 mM PIPES pH 8.0, 85 mM KCl, 0.5% NP-40

plus protease inhibitors) passed ten times through a 21G syringe needle. Nuclei were pelleted and

resuspended in (1% NP-40, 0.5% Na deoxycholate, 0.1% SDS in PBS containing protease inhibitors) and

chromatin was sonicated to an average size of approximately 500bp. Chromatin immunoprecipitations

were performed with rabbit anti-TOP2A 4566, rabbit anti-TOP2B 4555 or control rabbit IgG pre-bound

to protein A Dynabeads (Thermo Fisher Scientific, UK). For semi-quantitative PCR analysis, cycle

numbers were chosen that resulted in near endpoint yield for inputs (diluted 30X compared to IP

samples) but clearly sub-endpoint yield for the test samples based on product band intensity and

remaining primer visible as a lower band on the agarose gels. PCR products were resolved on 2%

agarose gels stained with GelRed. For real-time QPCR reactions were performed using Ciba green and

a Biorad CFX96 PCR machine using the ΔΔCt method. ChIP PCR primers have been described previously

and were as follows: R-Prom f-GAGGACAGCGTGTCAGCAATAA, r-GCCCCGGGGGGAGGTAT; FY-42 f-

CTTTCCGGAGCTCTGCCTAG, r-GGTTGTCGGGCTCCATCT; OS-H4 f-CTCTCCGGAATCGAACCCTGA, r-

CGACGACCCATTCGAACGTCT; OS-H8 f-CCCTTACGGTACTTGTTGACT, r-AGTCGGGTTGCTTGGGAATGC;

OS-H18 f-GGAAGTTGTCTTCACGCCTGA, r-GTTGACGTACAGGGTGGACTG; Sa-GB f-

AAGGTCAATGGCAGAAAAGAA, r-CAACGAAGGCCACAAGATGTC; Sa-GB f-

MOL # 117390

AAGGTCAATGGCAGAAAAGAA, r-CAACGAAGGCCACAAGATGTC (O'Sullivan *et al.*, 2002; Ray *et al.*, 2013; Yu *et al.*, 2015).

Data analysis

Statistical analysis was performed using Graph Pad Prism 8.2. The details of the tests performed are given in figure legends. For signifying *P* values, * refers to P < 0.05, ** refers to *P* < 0.01,*** refers to *P*< 0.001 and **** refers to *P*<0.0001. Error bars in bar charts represent SD values. The study was designed to be exploratory rather than testing a specific null hypothesis and p value are therefore descriptive only. Sample sizes (numbers of replicate experiments) were specified in advance of data acquisition based on prior knowledge of the characteristics of the assays involved and anticipating occasional lost or failed samples.

Results

PR-619 induces TOP2A and TOP2B covalent DNA complexes. TOP2-DNA covalent complexes stabilised by drugs such as etoposide can be visualised and quantified using the TARDIS assay which allows immunofluorescent analysis after removing cellular proteins, including histones, by high stringency extraction of cells embedded in agarose leaving nuclear ghosts of genomic DNA in situ (Supplemental Fig. 1A-C). We had observed that etoposide-induced TOP2 DNA covalent complexes detected using this assay are accompanied by ubiquitin and SUMO immunofluorescence signal (Supplemental Fig. 1B&C). When carrying out experiments to examine the ubiquitination of TOP2 in covalent DNA complexes, we noticed that the broad-spectrum DUB inhibitor PR-619 (Altun *et al.*, 2011) itself induced both TOP2A and TOP2B-DNA covalent complexes (Fig. 1 and Supplemental Fig. 2 A&B bottom six panels). As is the case for etoposide, PR-619 at 40μM induced an above-background TOP2A and TOP2B signal in nearly all cells (Supplemental Fig. 2A&B). For TOP2A the median signal intensity induced by 80μM PR-619 was approximately half that obtained with 100μM Etoposide and

9

for TOP2B the figure was 75% (Fig. 1). By contrast, at 10µM PR-619 did not induce detectable TOP2A complexes (Fig. 1, Supplemental Fig. 2C). Under standard TARDIS conditions TOP2A complexes are almost undetectable in non-drug-treated cells, whereas TOP2B reproducibly gives a small above zero signal in untreated cells, presumably reflecting the capture of endogenous TOP2B activity. Although PR-619 induced a clear induction of TOP2B complexes at 20, 40 and 80µM, little if any increase in TOP2B signal above that observed in untreated cells was observed in cells treated with 10µM PR-619 (Fig 1, middle panel, Supplemental Fig. 1C). As described above, it is possible to analyse TOP2 post-translational modifications using the TARDIS assay as the cell lysis and slide processing removes cellular constituents not covalently attached to genomic DNA. Using pan-ubiquitin antibodies, this revealed that at least some TOP2-DNA complexes induced by etoposide are ubiquitinated (Supplemental Fig. 1B, & 2). Cells treated with 20, 40 or 80 µM PR-619 exhibited a much higher ubiquitin signal than those treated with etoposide (Fig. 2 right-hand panel and Supplemental Fig. 2), consistent with the activity of PR-619 as a DUB inhibitor. This leads to the conclusion that for complexes induced by PR-619 a higher proportion of the TOP2 molecules are ubiquitinated or that each TOP2 complex is ubiquitinated to a greater extent than those induced by etoposide. Notably, even at 10µM PR-619 some cells exhibited a high ubiquitin signal, although most nuclei remained at the untreated level (Supplemental Fig. 1C rh panel). This is surprising given that at this concentration PR-619 induced little if any additional TOP2A or TOP2B fluorescence above that observed in untreated cells but could be explained if 10µM PR-619 treatment results in hyper-ubiquitination of endogenous (i.e. non-drug induced) TOP2B complexes. Thus, PR-619 behaves as an effective TOP2 poison, at a similar dose range as etoposide.

Induction of TOP2 DNA covalent complexes by PR-619 is not due to hyperubiquitination of TOP2

Since PR-619 is a broad range DUB inhibitor and treatment with PR-619 resulted in bright labelling of nuclear ghosts with anti-ubiquitin as well at TOP2 antibodies (Supplemental Fig. 1 B&C and Fig. 1 right hand panels), we hypothesised that the induction of TOP2-DNA complexes by PR-619 could be linked

to its DUB inhibitory activity. To test this hypothesis we pre-treated cells with the E1 ubiquitin

activating enzyme (UAE) inhibitor MLN7243 at a dose and time previously shown to cause a loss of

polyubiquitin chains and of monoubiquitinated histone H2A in cells (Hyer *et al.*, 2018). As expected,

this pre-treatment greatly reduced the accumulation of ubiquitin in nuclear ghosts formed from PR-

619 treated cells (Fig. 1 rh panel). However, contrary to expectations, ubiquitin depletion by MLN7243

had no significant effect on PR-619-induced TOP2A or TOP2B complexes. MLN7243 did not induce

TOP2-DNA complexes on its own, and also had no effect on etoposide-induced TOP2-DNA complex

formation (Fig. 1 left and middle panels). Thus, PR-619 acts as a TOP2 poison independently of the

effects of DUB inhibition. This conclusion is supported by *in vitro* enzyme assays where, like etoposide,

PR-619 stimulated TOP2A and TOP2B plasmid cleavage activity and inhibited decatenation activity

(Fig. 2).

Etoposide treatment results in SUMO2/3 accumulation that coincides with TOP2 signal in the TARDIS

assay (Schellenberg *et al.*, 2017; Lee *et al.*, 2018) (Supplemental Fig. 1C). Since PR-619 has been shown

to inhibit sentrin-specific proteases (SENPs) (Altun *et al.*, 2011) we were interested to determine

whether PR-619 induced a proportionally greater level of SUMOylated protein-DNA covalent

complexes. As shown in Supplemental Fig. 3A-C, PR-619 did induce a robust SUMO2/3 signal which

coincided with the nuclear signal intensity observed for TOP2A and TOP2B, consistent with the

presence of SUMOylated TOP2 complexes. However, we were not able to efficiently suppress the level

of sumoylation induced by PR-619 using small molecule inhibitors 2-DO8 or ML-792, which affect the

transfer of SUMO from the E2 enzyme UBC9 or SAE1 activity respectively (Kim *et al.*, 2013; He *et al.*,

2015).

PR-619 induced TOP2A and TOP2B covalent complexes that are unevenly distributed in the nucleus.

We routinely observe that etoposide and other established TOP2 poisons such as mitoxantrone induce

TOP2A and TOP2B fluorescence signal throughout the volume of the nuclear ghosts in the TARDIS

assay, although this can appear slightly granular for TOP2B under higher magnification widefield microscopy (Fig. 3A&B). However, in most cells PR-619 induced a different distribution of TOP2A and TOP2B fluorescent signal consisting of large foci of signal (Fig. 3A&B). The FK2 ubiquitin fluorescent signal partially overlapped that of both TOP2A and TOP2B (Fig. 3), as did that for SUMO2/3 (Supplemental Fig. 3A), consistent with the conclusion that the bright ubiquitin and SUMO signals originate from ubiquitinated and SUMOylated TOP2 trapped as covalent-DNA complexes.

PR-619 drives ubiquitin-independent nucleolar localization of TOP2A and TOP2B.

Historically there has been some disagreement regarding the sub-nuclear distribution of pools of TOP2, especially TOP2B, probably due to the use of cells from different species, different antibodies and different fixation conditions (Chaly and Brown, 1996; Onoda *et al.*, 2014; Austin *et al.*, 2018). The consensus, in agreement with our own observations, is that TOP2 is mobile in the interphase nucleus and is distributed throughout the nucleoplasm with some distribution in the nucleoli. In addition we have also observed concentration of TOP2B in the abundant perinucleolar heterochromatin of mouse cells (Cowell *et al.*, 2011). Thus, we were interested to determine whether the uneven focal distribution of PR-619-induced TOP2A and TOP2B-DNA complexes in TARDIS assays reflected nucleolar concentration of TOP2. The harsh lysis conditions employed in the TARDIS assay remove proteinaceous nuclear structures, precluding co-staining for nucleolar markers such as fibrillarin or pol I. So, we examined the distribution of TOP2A and TOP2B in PR-619 treated K562 cells by standard immunofluorescence using paraformaldehyde fixation at room temperature. Under these fixation conditions both TOP2A and TOP2B display a fairly even nucleoplasm staining pattern in the majority of interphase cells. In contrast, in PR-619-treated cells TOP2A and TOP2B became concentrated in a few large nuclear foci, reminiscent of the pattern observed under TARDIS conditions (Fig. 3, Fig. 4A&B). Co-staining for TOP2A or TOP2B and fibrillarin confirmed that the large focal TOP2 clusters in PR-619 colocalised with nucleoli (Fig. 4B). PR-619 induced a large increase in overall protein ubiquitination, as detected using antibody FK2 in paraformaldehyde fixed cells, but prior treatment with the UAE

inhibitor MLN7243 resulted in almost complete loss of FK2 signal, even in PR-619 treated cells (Fig 4C). However, the PR-619 associated nucleolar redistribution of TOP2 was not affected by prior treatment with the MLN7423. Thus, the nucleolar redistribution of TOP2A and TOP2B in PR-619 treated cells does not appear to be dependent on hyperubiquitination of the enzymes.

Sites of TOP2 activity can be visualised using the Differential Retention of TOP2 (DRT) assay (Agostinho *et al.*, 2004), in which adherent cells grown on coverslips are extracted with salt and detergent to enrich for active TOP2 molecules that are trapped on DNA. Since overall nuclear architecture is better conserved by DRT than in the TARDIS assay, this method was used to examine the nuclear distribution of active TOP2A and TOP2B in HeLa cells. In the absence of added drug, most TOP2A and TOP2B was lost from the cells, as expected (Supplemental Figs 4 & 5, top rows). However, PR-619 treatment led to the formation of focal concentrations of both TOP2A and TOP2B corresponding to the location of nucleoli as judged from the DAPI staining pattern. In contrast, but consistent with previous observations, etoposide induced an essentially pan-nuclear TOP2A pattern and a fine granular pattern with TOP2B. Thus, PR-619 traps TOP2A and TOP2B in the nucleolar compartment of the epithelial cells (HeLa) as well as lymphoblastoid cells (K562). In order to be trapped and stable to extraction, TOP2 must presumably be active in the nucleolar compartment of PR-619-treated cells. Notably, Onada et al have demonstrated that a pool of TOP2B is localised in the nucleolar regions in live cells and after fixing with formaldehyde at 37℃, but redistributes to the nucleoplasm if cells are cooled, and report that this nucleolar pool is largely inactive and bound to RNA (Onoda *et al.*, 2014). To determine whether TOP2 is concentrated in the nucleolar domain via RNA interactions in PR-619 treated cells, K562 cells were treated with PR-619 or etoposide and TOP2 complexes were visualised and quantified using the TARDIS assay after treating extracted agarose-embedded cells with RNaseA. Notably, RNase treatment made no difference to either the qualitative distribution or the intensity of the TOP2A or TOP2B signals (Supplemental Fig. 6).

Since etoposide and PR-619 induce TOP2-DNA complexes with different distributions in the nucleus, we carried out combination experiments to determine whether complex formation would be

13

quantitatively (in the overall level of complexes formed) or qualitatively (in the distribution of TOP2 complexes in the nucleus) additive. Using both drugs at concentrations that individually generate similar levels of TOP2 complexes (50µM Etoposide, 80µM PR-619) we found that for TOP2B, combination of both drugs resulted in an approximately 30% larger signal than either drug alone, whether the drugs were added simultaneously or sequentially (Fig. 5A). For TOP2A, the combination resulted in only a marginal increase in signal compared to PR-619 alone (Fig. 5A). Thus, there is some additive effect, particularly for TOP2B, but this may have been limited by saturating effects at the concentrations of drugs used. While etoposide and PR-619 treatment resulted in different distributions of TOP2A and TOP2B within nuclear ghosts (Fig. 5B) combined treatment with both drugs resulted in TOP2A and TOP2B complex distributions very similar to that obtained with PR-619 alone (Fig. 5B, Supplemental Figs 7 & 8). In particular, pre-treatment with etoposide did not noticeably prevent the focal distribution associated with PR-619, suggesting that a sufficient pool of un-trapped TOP2 remains after 50µM etoposide treatment to subsequently give rise to the focal PR-619-derived pattern of TOP2 complexes. Also of note, pre-treatment with 5µM PR-619, sufficient to inhibit DUB and SENP activity (Altun *et al.*, 2011) but insufficient to generate TOP2-DNA complexes did not affect the distribution of TOP2 complexes induced by etoposide.

TOP2A and TOP2B associate with rDNA repeats

Given that PR-619 treatment leads to nucleolar retention of TOP2 (Fig. 4) and induces TOP2-DNA complexes that appear to coincide with nucleolar derived regions in TARDIS and DRT assays, we set out to determine whether PR-619 drives TOP2 association with rDNA repeats. Notably previous studies have demonstrated that TOP2B is present across at least some rDNA repeat units by ChIP-seq (Uusküla-Reimand *et al.*, 2016) and that TOP2A associates with and promotes the activity of pol I at rDNA promoters (Ray *et al.*, 2013). We performed ChIP analysis with brief formaldehyde crosslinking and utilizing PCR primers corresponding to the rDNA promoter, 18S and 28S coding regions and the spacer region (Fig. 6A). Under control conditions TOP2A and TOP2B could be detected at each of these

14

locations using semi-quantitative PCR, but the signal was more robust with either TOP2 poison, particularly with PR-619 (Fig. 6B). This was confirmed by QPCR for two of the locations (promoter and 28S, Fig. 6C). Thus, PR-619 does appear to lead to increased association of TOP2A and TOP2B with rDNA. For comparison, we examined the association of TOP2 with satellite DNA (some of which occupies a perinucleolar position in the nucleus) using an alpha satellite PCR primer pair. We observed a robust TOP2A and TOP2B ChIP signal under each condition but did not observe additional PR-619 mediated accumulation for alpha satellite DNA (Fig. 6B).

PR-619 efficiently induces histone H2AX phosphorylation.

Cellular processing of TOP2-DNA complexes via proteasomal destruction and other mechanisms leads to the appearance of protein-free DSBs which are otherwise concealed by TOP2 protein and do not elicit a DNA damage response (Mårtensson *et al.*, 2003; Zhang *et al.*, 2006; Fan *et al.*, 2008; Schellenberg *et al.*, 2017; Lee *et al.*, 2018). As a proxy for DSBs, we measured the appearance of phospho-histone H2AX (γH2AX) in K562 cells treated with etoposide or PR-619. Both etoposide and PR-619 induced robust H2AX phosphorylation at doses that efficiently trap TOP2 in covalent-DNA complexes (Fig. 7A-C, Supplemental Fig. 9,). However, comparing equal doses of PR-619 and etoposide, PR-619 exhibited a much steeper dose response than etoposide, producing little γH2AX in most cells at 20μM and background levels at 5 and 10μM.

PR-619 induces persistent TOP2-DNA complexes.

The resolution of poison-induced TOP2-DNA covalent complexes in cells after drug washout can be followed using the TARDIS, ICE or potassium-SDS precipitation assays (Hsiang and Liu, 1989; Errington *et al.*, 2004; Nitiss *et al.*, 2012; Schellenberg *et al.*, 2017). In cultured mammalian cells, the half-life of etoposide-induced TOP2A and TOP2B complexes is less than an hour (Errington *et al.*, 2004; Schellenberg *et al.*, 2017). However, the observed reversal rate differs for different TOP2 poisons. While the mAMSA reversal rate is similar to etoposide, it is much longer for mitoxantrone (Fox and

MOL # 117390

Smith, 1990; Willmore *et al.*, 2002), and in the case of the anthracycline idarubicin, we observed TOP2-covalent DNA complexes increase for up to 48 hours after drug washout (Errington *et al.*, 2004). To determine the longevity of PR-619-induced TOP2 complexes K562 cells were incubated with etoposide or PR-619 for two hours as before, and then collected for TARDIS analysis before and after drug washout (1hr) and re-plating in fresh medium. In line with the rapid reversal of etoposide-induced TOP2 DNA complexes observed previously, most of the etoposide-induced TOP2A signal was lost and TOP2B complexes returned to background levels following drug washout. In contrast, in K562 cells treated with PR-619, TOP2A and TOP2B signals increased significantly following drug washout, while the ubiquitin signal was maintained (Fig. 8A&B). The reason for the persistence of the PR-619-induced complexes could include slower cellular processing of these complexes compared to those induced by etoposide; however the appearance of abundant γH2AX (similar to the signal obtained with 50μM etoposide) during the two-hour dug incubation period (Figs 7 & Supplemental Fig. 9) indicates that a substantial fraction of PR-619-induced TOP2 complexes are processed to reveal protein-free breaks during this period. Alternatively, greater retention of PR-619 in K562 cells following drug washout could lead to persistence of TOP2-DNA complexes, an explanation that has been suggested for the persistence of mitoxantrone and idarubicin induced TOP2-DNA complexes (Willmore *et al.*, 2002; Errington *et al.*, 2004). In this scenario significant PR-619 is retained in cells during drug washout, resulting in continued formation of new TOP2-DNA complexes even as the initial complexes are processed to DSBs. In support of this, the yellow colour of PR-619 was clearly visible in cell pellets of PR-619 treated cells after washing with PBS.

Discussion

We have demonstrated that PR-619, a previously characterised broad spectrum DUB inhibitor (Altun *et al.*, 2011) is also a TOP2 poison, inducing TOP2A and TOP2B DNA complexes with similar potency to the "archetypal" and clinically important TOP2 poison etoposide. Established TOP2 poisons fall into a

number of chemical classes including podophyllotoxins such as etoposide and teniposide, the anthraciendiones mitoxantrone and pixantrone, anthracyclines such as idarubicin, acridines including *m*AMSA, and the quinolone Voreloxin (Pommier *et al.*, 2010). However, PR-619 (2,6-diaminopyridine-3,5-bis(thiocyanate)) is chemically distinct from each of these classes of TOP2 poison. TOP2-DNA complexes induced by PR-619 were highly ubiquitinated. However, TOP2-DNA covalent complexes were formed in PR-619 treated cells even in the presence of UAE inhibitor MLN7243, although the level of ubiquitination of the complexes was much lower in MLN7243 pre-treated cells. Thus, it does not appear that hyperubiquitination of TOP2A or TOP2B is a prerequisite for the formation of TOP2-DNA complexes. In a previous study using HCT-116 cells (Hyer *et al.*, 2018), and as demonstrated here in K562 cells (Fig. 5C), MLN7243 causes a very large reduction in protein ubiquitination within 2 hours (the length of pre-incubation employed in this study). So, it is unlikely, though cannot be fully excluded, that hyperubiquitination of another protein interferes with normal TOP2 activity leading to TOP2-DNA complex formation. We found TOP2 complexes induced by etoposide are decorated with SUMO2/3 in addition to ubiquitin (Supplemental Figs 1C & 3), as observed previously (Agostinho *et al.*, 2008; Schellenberg *et al.*, 2017; Lee *et al.*, 2018); but the intensity of SUMO staining was greater in PR-619 treated cells, consistent with the activity of the inhibitor against SENPs. Thus, it is plausible that PR-619 induces TOP2 complexes via hyperSUMOylation of the enzymes or another cellular component. We were unable to fully exclude this possibility in cell-based studies as pre-treatment with neither 2-D08 nor ML-792 substantially affected the SUMO2/3 signal induced in nuclear ghosts by PR-619 (Supplemental Figure 3). However, since PR-619 induced DNA cleavage and inhibited relaxation activities of TOP2A and TOP2B in *in vitro* cleavage assays (Fig. 2) PR-619 induced formation of TOP2A and TOP2B-DNA complexes in cells is likely to be a direct action on TOP2 enzyme activity. In addition to inducing TOP2-DNA complexes, PR-619 uniquely caused a redistribution of TOP2 into the nucleolar compartment, observed by standard immunofluorescence employing paraformaldehyde fixation and in TARDIS imaging. This phenomenon occurred even when cells were pre-treated with MLN7243, and so also appears to be independent of the DUB inhibitor activity of PR-619. However,

for the reasons described above, we are not able to exclude the possibility that hyperSUMOylation of TOP2 contributes to its nucleolar accumulation. However, arguing against this, we observed that PR-619 at a concentration (5-10µM) that achieves efficient DUB and SENP inhibition in cells (Altun *et al.*, 2011) did not affect the diffuse nuclear distribution of etoposide-induced TOP2-DNA complexes (Fig. 5). Notably though, SUMOylation of TOP2 is associated with targeting to mitotic chromosomes (Azuma *et al.*, 2005; Agostinho *et al.*, 2008) and artificial fusion of poly-SUMO to yeast Top2 results in nucleolar targeting (Takahashi and Strunnikov, 2008). Although TOP2A and TOP2B are found throughout the interphase nucleus by immunofluorescence in fixed cells they are both components of the nucleolar proteome (Andersen *et al.*, 2005). In addition, protein interactions between TOP2B and a number of nucleolar proteins have been demonstrated (Uusküla-Reimand *et al.*, 2016) and live cell imaging revealed a dynamic and more nucleolar distribution of TOP2A and TOP2B GFP fusion proteins (Christensen *et al.*, 2002; Onoda *et al.*, 2014). Thus, it is reasonable to conclude that PR-619 influences the normal distribution of TOP2 between the nucleoplasm and nucleoli, although the mechanism behind this is currently unclear. Notably, in order to form complexes resistant to extraction in TARDIS and DRT assays TOP2A and TOP2B must be enzymatically active in the nucleolar compartment in PR-619 treated cells. TOP2A and TOP2B have been reported to associate with rDNA sequences and in ChIP-seq analysis TOP2B occupancy was evident across the rDNA repeat unit coding region and at the promoter and adjacent CTCF binding region (Ray *et al.*, 2013; Uusküla-Reimand *et al.*, 2016). Although we could detect TOP2A and TOP2B at the promoter and coding regions of the rDNA repeat unit in untreated cells even with the relatively mild crosslinking conditions employed (Fig. 6B), ChIP efficiency was greater when TOP2 was trapped on DNA by etoposide, or PR-619, but this effect was more robust in the case of PR-619 (Fig. 6 B&C). This is consistent with PR-619 resulting in abundant TOP2-DNA complexes within rDNA repeat units, although our evidence suggests that these complexes are distributed across the locus.

PR-619 has become a useful tool to probe the role of ubiquitination in various cell biological systems (Balut *et al.*, 2011; Seiberlich *et al.*, 2012; Pandey and Kumar, 2015; Crowder *et al.*, 2016; Rana *et al.*, 2017; Wang *et al.*, 2017), but the work here suggests that some caution should be applied when using this inhibitor in cell line based studies. We have observed that at concentrations 20µM and above, PR-619 induces TOP2 covalent DNA complexes in K562 cells that are converted to DNA double strand breaks. Notably, the concentration range where we have observed pronounced TOP2 poison activity and γH2AX induction in K562 cells (20-80µM) is higher than the lowest concentrations for which PR-619 has demonstrated robust DUB inhibitory activity (5-20µM) and growth inhibitory activity (IC_{50} ~2µM) in HEK293T cells (Altun *et al.*, 2011). Thus, the additional TOP2 poisoning property of PR-619 can be avoided by careful consideration of concentration.

Acknowledgements

Author contributions

Participated in research design: Swan, Austin, Cowell

Conducted experiments: Cowell, Swan, Ling, Brooks, Austin

Performed data analysis: Cowell

Wrote or contributed to writing manuscript: Cowell

References

Agostinho M, Rino J, Braga J, Ferreira F, Steffensen S, and Ferreira J (2004) Human topoisomerase IIalpha: targeting to subchromosomal sites of activity during interphase and mitosis. *Mol Biol Cell* **15**:2388–2400.

Agostinho M, Santos V, Ferreira F, Costa R, Cardoso J, Pinheiro I, Rino J, Jaffray E, Hay RT, and Ferreira J (2008) Conjugation of Human Topoisomerase 2α with Small Ubiquitin-like Modifiers 2/3 in Response to Topoisomerase Inhibitors: Cell Cycle Stage and Chromosome Domain Specificity. *Cancer Res* **68**:2409–2418.

Altun M, Kramer HB, Willems LI, McDermott JL, Leach CA, Goldenberg SJ, Kumar KGS, Konietzny R, Fischer R, Kogan E, Mackeen MM, McGouran J, Khoronenkova SV, Parsons JL, Dianov GL, Nicholson B, and Kessler BM (2011) Activity-Based Chemical Proteomics Accelerates Inhibitor Development for Deubiquitylating Enzymes. *Chem Biol* **18**:1401–1412.

Andersen JS, Lam YW, Leung AKL, Ong S-E, Lyon CE, Lamond AI, and Mann M (2005) Nucleolar proteome dynamics. *Nature* **433**:77–83.

Atwal M, Swan RL, Rowe C, Lee KC, Lee DC, Armstrong L, Cowell IG, and Austin CA (2019) Intercalating TOP2 poisons attenuate topoisomerase action at higher concentrations. *Mol Pharmacol* mol.119.117259.

Austin C, Lee K, Swan R, Khazeem M, Manville C, Cridland P, Treumann A, Porter A, Morris N, Cowell I, Austin CA, Lee KC, Swan RL, Khazeem MM, Manville CM, Cridland P, Treumann A, Porter A, Morris NJ, and Cowell IG (2018) TOP2B: The First Thirty Years. *Int J Mol Sci* **19**:2765.

Azuma Y, Arnaoutov A, Anan T, and Dasso M (2005) PIASy mediates SUMO-2 conjugation of Topoisomerase-II on mitotic chromosomes. *EMBO J* **24**:2172–2182.

Balut CM, Loch CM, and Devor DC (2011) Role of ubiquitylation and USP8-dependent deubiquitylation in the endocytosis and lysosomal targeting of plasma membrane KCa3.1. *FASEB J* **25**:3938–3948.

Barry R, John SW, Liccardi G, Tenev T, Jaco I, Chen C-H, Choi J, Kasperkiewicz P, Fernandes-Alnemri T, Alnemri E, Drag M, Chen Y, and Meier P (2018) SUMO-mediated regulation of NLRP3 modulates inflammasome activity. *Nat Commun* **9**:3001.

Burden DA, Froelich-Ammon SJ, and Osheroff N (2001) Topoisomerase II-mediated cleavage of plasmid DNA. *Methods Mol Biol* **95**:283–289.

Chaly N, and Brown DL (1996) Is DNA topoisomerase II beta a nucleolar protein? *J Cell Biochem* **63**:162–173.

Christensen MO, Larsen MK, Barthelmes HU, Hock R, Andersen CL, Kjeldsen E, Knudsen BR, Westergaard O, Boege F, and Mielke C (2002) Dynamics of human DNA topoisomerases IIalpha and IIbeta in living cells. *J Cell Biol* **157**:31–44.

Cowell IG, and Austin CA (2012) Mechanism of generation of therapy related leukemia in response to anti-topoisomerase II agents. *Int J Environ Res Public Health* **9**:2075–2091.

Cowell IG, and Austin CA (2018) Visualization and Quantification of Topoisomerase-DNA Covalent Complexes Using the Trapped in Agarose Immunostaining (TARDIS) Assay. *Methods Mol Biol* **1703**:301–316.

Cowell IG., Papageorgiou N, Padget K, Watters GP, and Austin CA (2011) Histone deacetylase inhibition redistributes topoisomerase IIβ from heterochromatin to euchromatin. *Nucleus* **2**:61–71.

Cowell IG., Tilby MJ, and Austin CA (2011) An overview of the visualisation and quantitation of low and high MW DNA adducts using the trapped in agarose DNA immunostaining (TARDIS) assay. *Mutagenesis* **26**:253–260.

Crowder RN, Dicker DT, and El-Deiry WS (2016) The Deubiquitinase Inhibitor PR-619 Sensitizes Normal Human Fibroblasts to Tumor Necrosis Factor-related Apoptosis-inducing Ligand (TRAIL)-mediated Cell Death. *J Biol Chem* **291**:5960–5970.

D'Arcy P, Wang X, and Linder S (2015) Deubiquitinase inhibition as a cancer therapeutic strategy. *Pharmacol Ther* **147**:32–54.

Errington F, Willmore E, Leontiou C, Tilby MJ, and Austin CA (2004) Differences in the longevity of topo IIα and topo IIβ drug-stabilized cleavable complexes and the relationship to drug sensitivity. *Cancer Chemother Pharmacol* **53**:155–162.

Fan J-R, Peng A-L, Chen H-C, Lo S-C, Huang T-H, and Li T-K (2008) Cellular processing pathways contribute to the activation of etoposide-induced DNA damage responses. *DNA Repair* **7**:452–463.

Fox ME, and Smith PJ (1990) Long-Term Inhibition of DNA Synthesis and the Persistence of Trapped Topoisomerase II Complexes in Determining the Toxicity of the Antitumor DNA Intercalators mAMSA and Mitoxantrone. *Cancer Res* **50**:5813–5818.

Harrigan JA, Jacq X, Martin NM, and Jackson SP (2018) Deubiquitylating enzymes and drug discovery: emerging opportunities. *Nat Rev Drug Discov* **17**:57–78.

He X, Riceberg J, Pulukuri SM, Grossman S, Shinde V, Shah P, Brownell JE, Dick L, Newcomb J, and Bence N (2015) Characterization of the Loss of SUMO Pathway Function on Cancer Cells and Tumor Proliferation. *PLoS ONE* **10**:e0123882.

Hsiang YH, and Liu LF (1989) Evidence for the reversibility of cellular DNA lesion induced by mammalian topoisomerase II poisons. *J Biol Chem* **264**:9713–9715.

Huang X, and Dixit VM (2016) Drugging the undruggables: exploring the ubiquitin system for drug development. *Cell Res* **26**:484–498.

Hyer ML, Milhollen MA, Ciavarri J, Fleming P, Traore T, Sappal D, Huck J, Shi J, Gavin J, Brownell J, Yang Y, Stringer B, Griffin R, Bruzzese F, Soucy T, Duffy J, Rabino C, Riceberg J, Hoar K, Lublinsky A, Menon S, Sintchak M, Bump N, Pulukuri SM, Langston S, Tirrell S, Kuranda M, Veiby P, Newcomb J, Li P, Wu JT, Powe J, Dick LR, Greenspan P, Galvin K, Manfredi M, Claiborne C, Amidon BS, and Bence NF (2018) A small-molecule inhibitor of the ubiquitin activating enzyme for cancer treatment. *Nat Med* **24**:186–193.

Kim YS, Nagy K, Keyser S, and Schneekloth JS (2013) An Electrophoretic Mobility Shift Assay Identifies a Mechanistically Unique Inhibitor of Protein Sumoylation. *Chem Biol* **20**:604–613.

Lee KC, Swan RL, Sondka Z, Padget K, Cowell IG, and Austin CA (2018) Effect of TDP2 on the Level of TOP2-DNA Complexes and SUMOylated TOP2-DNA Complexes. *Int J Mol Sci* **19**:2056.

Lee MP, Sander M, and Hsieh TS (1989) Single strand DNA cleavage reaction of duplex DNA by Drosophila topoisomerase II. *J Biol Chem* **264**:13510–13518.

Manasanch EE, and Orlowski RZ (2017) Proteasome inhibitors in cancer therapy. *Nat Rev Clin Oncol* **14**:417–433.

Mårtensson S, Nygren J, Osheroff N, and Hammarsten O (2003) Activation of the DNA-dependent protein kinase by drug-induced and radiation-induced DNA strand breaks. *Radiat Res* **160**:291–301.

Nitiss JL, Soans E, Rogojina A, Seth A, and Mishina M (2012) Topoisomerase Assays. *Curr Protoc Pharmacol* **Chapter 3**:Unit3.3.

Onoda A, Hosoya O, Sano K, Kiyama K, Kimura H, Kawano S, Furuta R, Miyaji M, Tsutsui K, and Tsutsui KM (2014) Nuclear dynamics of topoisomerase IIβ reflects its catalytic activity that is regulated by binding of RNA to the C-terminal domain. *Nucleic Acids Res* **42**:9005–9020.

O'Sullivan AC, Sullivan GJ, and McStay B (2002) UBF Binding In Vivo Is Not Restricted to Regulatory Sequences within the Vertebrate Ribosomal DNA Repeat. *Mol Cell Biol* **22**:657–668.

Pandey V, and Kumar V (2015) Stabilization of SIRT7 deacetylase by viral oncoprotein HBx leads to inhibition of growth restrictive RPS7 gene and facilitates cellular transformation. *Sci Rep* **5**.

Pommier Y, Leo E, Zhang H, and Marchand C (2010) DNA Topoisomerases and Their Poisoning by Anticancer and Antibacterial Drugs. *Chem Biol* **17**:421–433.

Rana ASJB, Ge Y, and Strieter ER (2017) Ubiquitin Chain Enrichment Middle-Down Mass Spectrometry (UbiChEM-MS) Reveals Cell-Cycle Dependent Formation of Lys11/Lys48 Branched Ubiquitin Chains. *J Proteome Res* **16**:3363–3369.

Ray S, Panova T, Miller G, Volkov A, Porter ACG, Russell J, Panov KI, and Zomerdijk JCBM (2013) Topoisomerase IIα promotes activation of RNA polymerase I transcription by facilitating pre-initiation complex formation. *Nat Commun* **4**:1598.

Schellenberg MJ, Lieberman JA, Herrero-Ruiz A, Butler LR, Williams JG, Muñoz-Cabello AM, Mueller GA, London RE, Cortés-Ledesma F, and Williams RS (2017) ZATT (ZNF451)–mediated resolution of topoisomerase 2 DNA-protein cross-links. *Science* **357**:1412–1416.

Seiberlich V, Goldbaum O, Zhukareva V, and Richter-Landsberg C (2012) The small molecule inhibitor PR-619 of deubiquitinating enzymes affects the microtubule network and causes protein aggregate formation in neural cells: Implications for neurodegenerative diseases. *Biochim Biophys Acta BBA - Mol Cell Res* **1823**:2057–2068.

Setz C, Friedrich M, Rauch P, Fraedrich K, Matthaei A, Traxdorf M, and Schubert U (2017) Inhibitors of Deubiquitinating Enzymes Block HIV-1 Replication and Augment the Presentation of Gag-Derived MHC-I Epitopes. *Viruses* **9**.

Takahashi Y, and Strunnikov A (2008) In vivo modeling of polysumoylation uncovers targeting of Topoisomerase II to the nucleolus via optimal level of SUMO modification. *Chromosoma* **117**:189–198.

Uusküla-Reimand L, Hou H, Samavarchi-Tehrani P, Rudan MV, Liang M, Medina-Rivera A, Mohammed H, Schmidt D, Schwalie P, Young EJ, Reimand J, Hadjur S, Gingras A-C, and Wilson MD (2016) Topoisomerase II beta interacts with cohesin and CTCF at topological domain borders. *Genome Biol* **17**.

Wang Y, Zhuang L, Chen X, Xu M, Li Z, and Jin Y (2017) Inhibition of deubiquitinases alters gamete ubiquitination states and sperm-oocyte binding ability in pigs. *Anim Reprod Sci* **187**:64–73.

Willmore E, Errington F, Tilby MJ, and Austin CA (2002) Formation and longevity of idarubicin-induced DNA topoisomerase II cleavable complexes in K562 human leukaemia cells. *Biochem Pharmacol* **63**:1807–1815.

Willmore E, Frank AJ, Padget K, Tilby MJ, and Austin CA (1998) Etoposide targets topoisomerase IIα and IIβ in leukemic cells: isoform-specific cleavable complexes visualized and quantified in situ by a novel immunofluorescence technique. *Mol Pharmacol* **54**:78–85.

Yu F, Shen X, Fan L, and Yu Z (2015) Analysis of histone modifications at human ribosomal DNA in liver cancer cell. *Sci Rep* **5**:18100.

Zhang A, Lyu YL, Lin C-P, Zhou N, Azarova AM, Wood LM, and Liu LF (2006) A Protease Pathway for the Repair of Topoisomerase II-DNA Covalent Complexes. *J Biol Chem* **281**:35997–36003.

Footnotes

Figure Legends

Figure 1. PR-619 induces TOP2 complexes in K562 cells with similar efficiency as etoposide, and complex formation is not dependent on ubiquitination. Cells were treated with PR-619, etoposide or solvent control. Where indicated cells were also treated with the E1 UEA inhibitor MNL7243 (10μM) prior to adding etoposide or PR-619. Cells were embedded in agarose on microscope slides and processed by TARDIS analysis for TOP2A, TOP2B and ubiquitin. Bar graphs represent the mean of the median values derived from replicates, which are also indicated individually as blue-lined circles. Error bars represent the SD . MNL7243 pre-treatment was for 2hr. Statistical analysis was performed using t-tests. For the last column in the left and right panel highlighted ($), cells were treated with 80μM PR-619 and processed with other samples, but with the omission of the primary antibody during immunofluorescence, to test for autofluorescence originating in the sample.

Fig. 2. PR-619 inhibits TOP2-induced DNA cleavage and relaxation of supercoiling in vitro. **(A)** Etoposide and PR619 induce plasmid cleavage by TOP2A or TOP2B. Plasmid cleavage was carried out with 600ng recombinant TOP2A (top) or 600 ng of recombinant TOP2B (bottom). Positions of nicked (N), linear (L), and supercoiled plasmid (SC) are denoted on the left. Linearized plasmid cleaved with EcoR1 is shown in lane 1. Substrate only and substrate with TOP2 (+T2) are shown in lanes 2 and 3 respectively. As a control, reactions with 1μL DMSO (lane 4) and 2μL DMSO (lane 13) are shown. **(B)** Etoposide and PR619 inhibited plasmid relaxation by TOP2A and TOP2B. Plasmid relaxation was carried out with 10 ng TOP2A (top) or 10 ng TOP2B (bottom). The positions of nicked (N), relaxed (R), and supercoiled plasmid (SC) are denoted on the left. Substrate only and substrate with TOP2 (+T2) are shown in lanes 1 and 2 respectively. As a control, reactions with 1μL DMSO (lane 3) and 2μL DMSO (lane 12) are included.

Figure 3. PR-619-induced TOP2 complexes are unevenly distributed in the nucleus. Cells were treated with PR-619, etoposide or solvent control (DMSO) for 2 hours and TOP2 complexes were

detected using the TARDIS assay. Immunofluorescence was performed using anti-TOP2A **(A)** or anti TOP2B **(B)** antibodies and anti-ubiquitin (FK2). Images were acquired using a 40X objective and are extended focus widefield images. Enlarged nuclei indicated by asterisk, bar=10μm.

Figure 4. PR-619 drives nucleolar localisation of TOP2A and TOP2B. K562 cells were treated with PR-619 (80μM) and where indicated were pre- treated with the UAE inhibitor MLN7243 (10μM, 2hr), fixed with paraformaldehyde and analysed by immunofluorescence for TOP2A **(A)** or TOP2B **(B)** and for the nucleolar marker fibrillarin. **(C)** K562 cells were treated as in A&B and stained for ubiquitin (FK2) and TOP2A. Images are shown as extended focus projections using 0.1μm z-steps and representative images obtained from several fields of cells from duplicate slides, bar=10μm.

Figure 5. Combined Etoposide and PR-619 treatment. K562 cells were treated with Etoposide or PR-619 individually for 150 minutes, with both for 150 min or with either one of the drugs first for 30 minutes before adding the other drug for 120 minutes and then collecting the cells for TARDIS analysis **(A)** Quantitative analysis of TARDIS samples as described for Fig. 1 **(B)** Representative nuclei from extended focus images acquired at higher magnification.

Figure 6. PR-619 treatment leads to enhanced association of TOP2A and TOP2B with rDNA. **(A)** Representation of the human rDNA repeat unit showing promoter (arrow), coding sequence (thick line), CTCF site (red bar) and PCR primers. **(B)** Semi-quantitative PCR from ChIP DNA samples from untreated (control), PR-619 treated and etoposide treated K562 cells. Track m: 100bp and 200bp markers, Input=1/30 dilution of input chromatin used for immunoprecipitation, IgG control rabbit IgG. Primer pair names and number of PCR cycles are indicated on the right. **(C)** Quantitative real time PRC analysis for primers R-prom (promoter) and OS-H8 coding region corresponding to 28S RNA.

Figure 7. PR-619 Induces histone H2AX phosphorylation. (A & B) K562 cells were treated with etoposide (50 μM) or PR-619 (80μM) for 2hr, fixed with paraformaldehyde and TOP2A or TOP2B and γH2AX was detected by immunofluorescences. Images are representative examples from three replica experiments. **(C)** H2AX phosphorylation per nucleus was assessed by quantitative immunofluorescent. Data represent the mean +/- SD, individual data points are indicated as blue-lined circles. Bar=10μm.

Figure 8. PR-619 induced TOP2 complexes persist after drug washout. K562 cells were incubated in the presence of Etoposide (40μM), PR-619 (80μM) or solvent (DMSO) for two hours. Cells were either collected immediately or drug was washed out and cells were re-plated and incubated for a further one hour before collection for TARDIS analysis. **(A)** Quantification of TARDIS data obtained using anti-TOP2A (4566), anti-TOP2B (4556) and anti-ubiquitin (FK2) antibodies. Median integrated fluorescence per nucleus values were normalised to the mean of the medians obtained with each drug directly after two hours incubation (i.e. without washout). Data are shown as mean values +/- SD and values from individual replicas are indicated as blue-lined circles. Statistical analysis, the normalised mean integrated fluorescence for PR-619 before and after washout were compared by unpaired t-test. **(B)** Representative images from TARDIS slides used to produce part A.
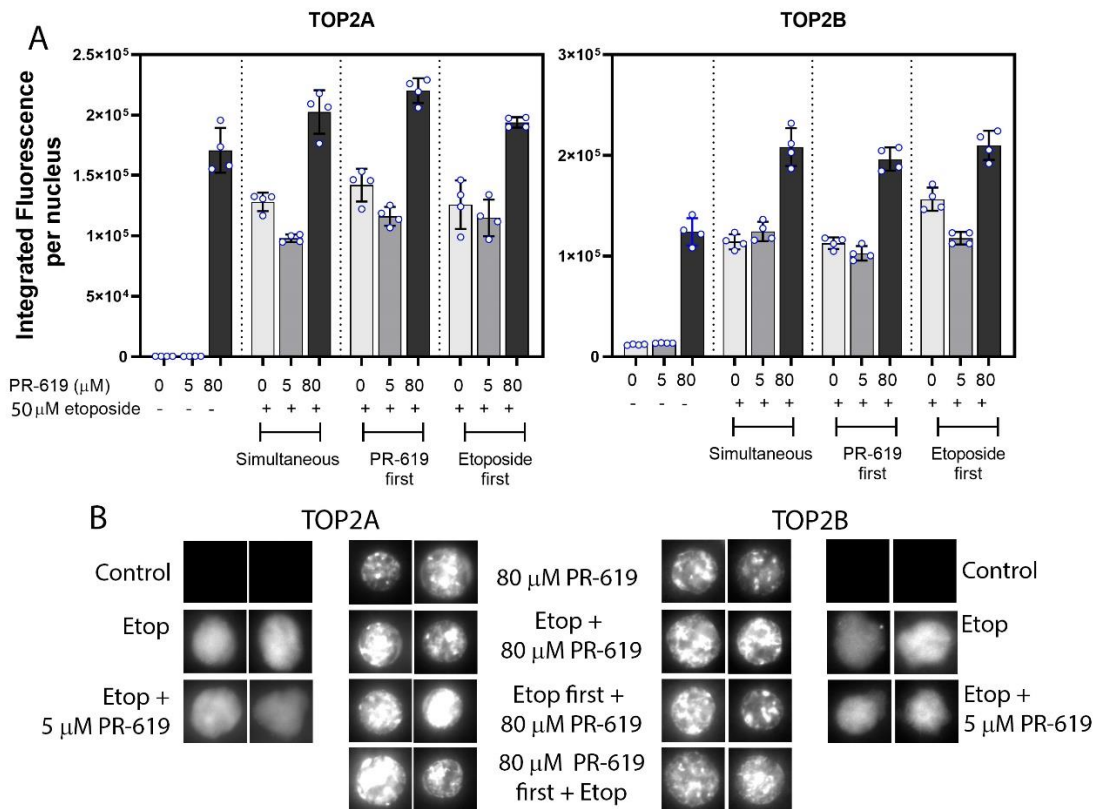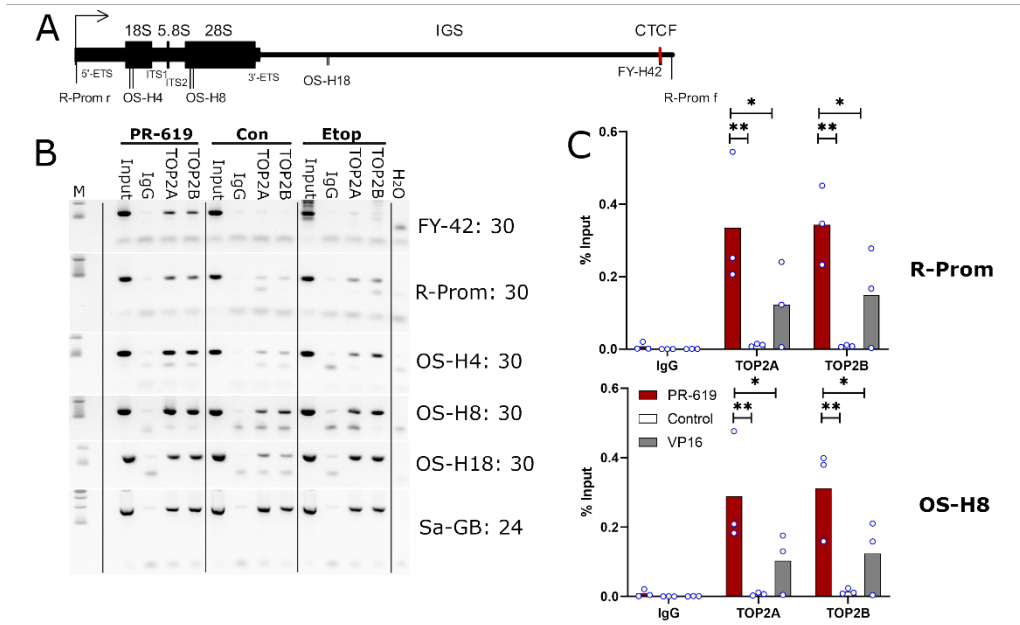
Figures
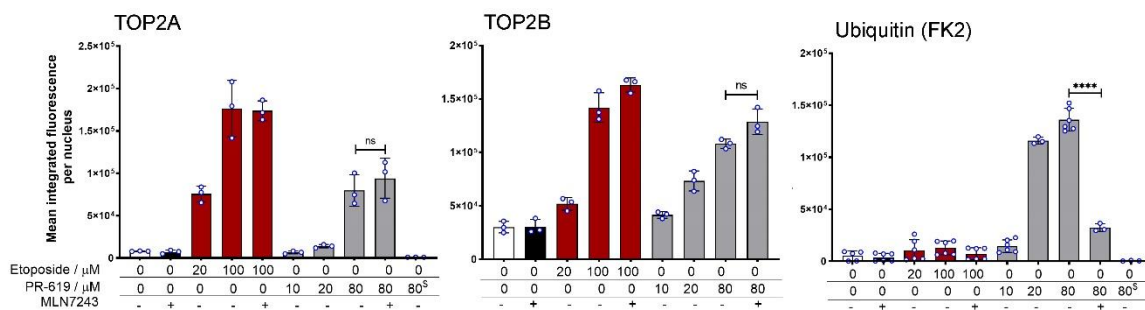
Figure 1
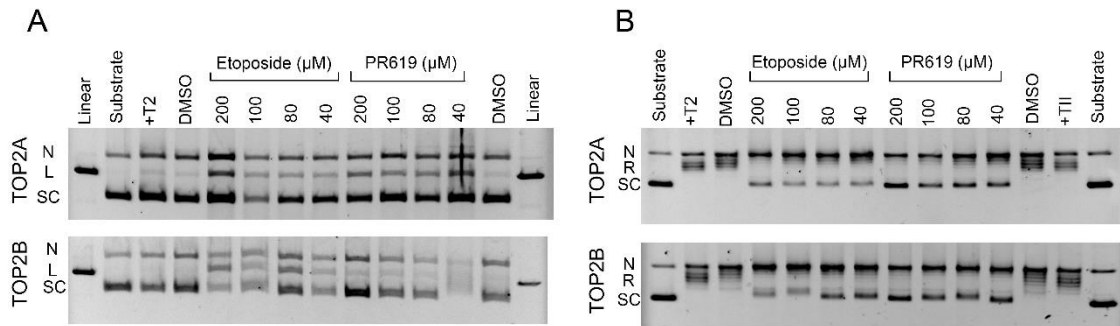
Figure 2
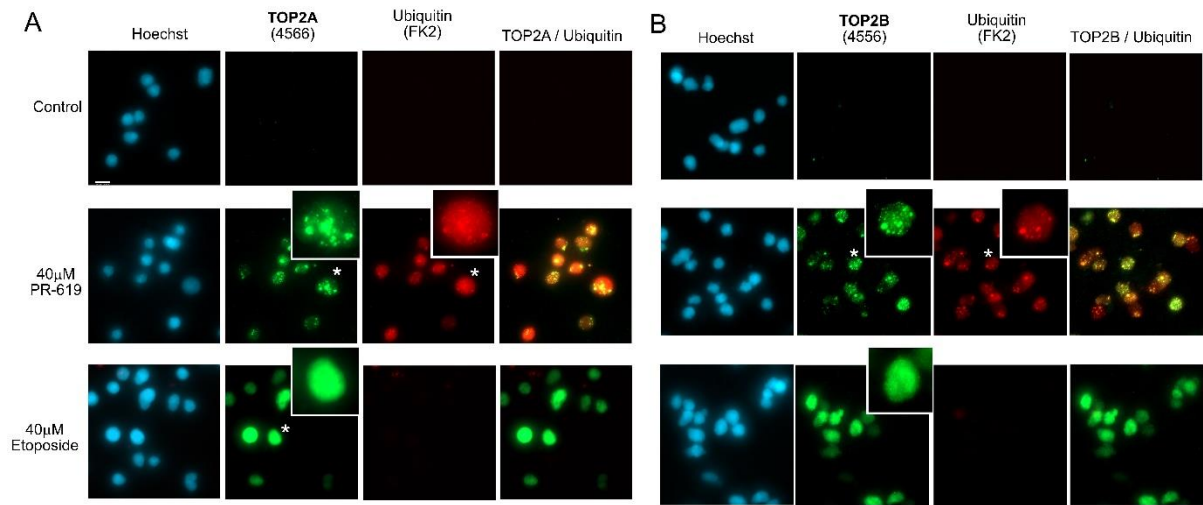
Figure 3
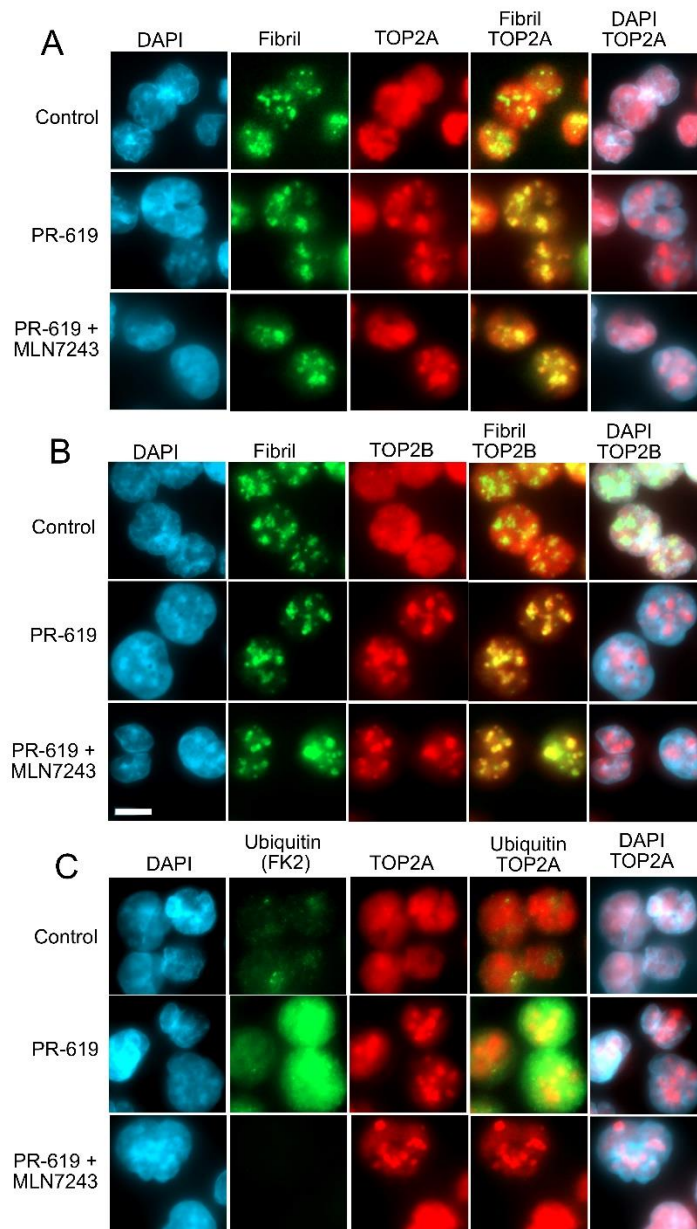
Figure 4

Figure 5

Figure 6

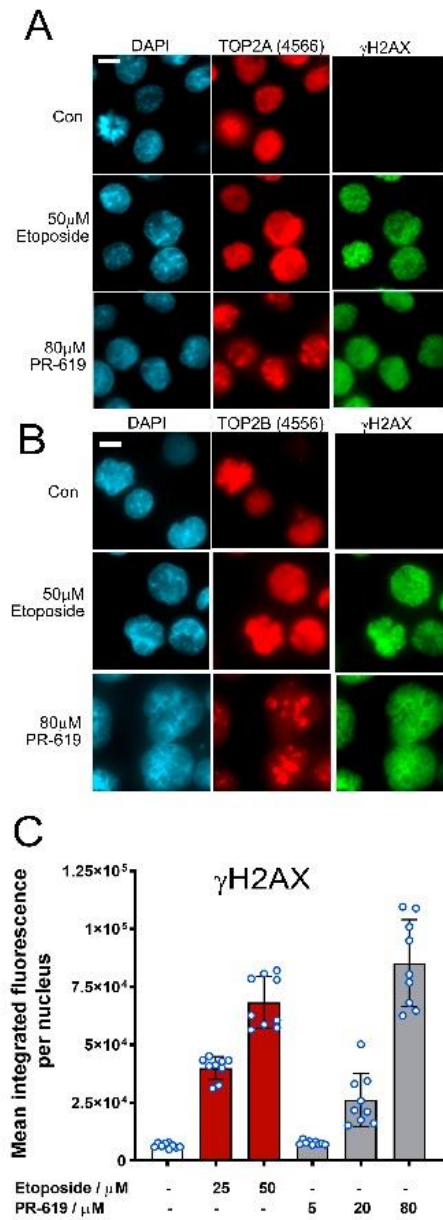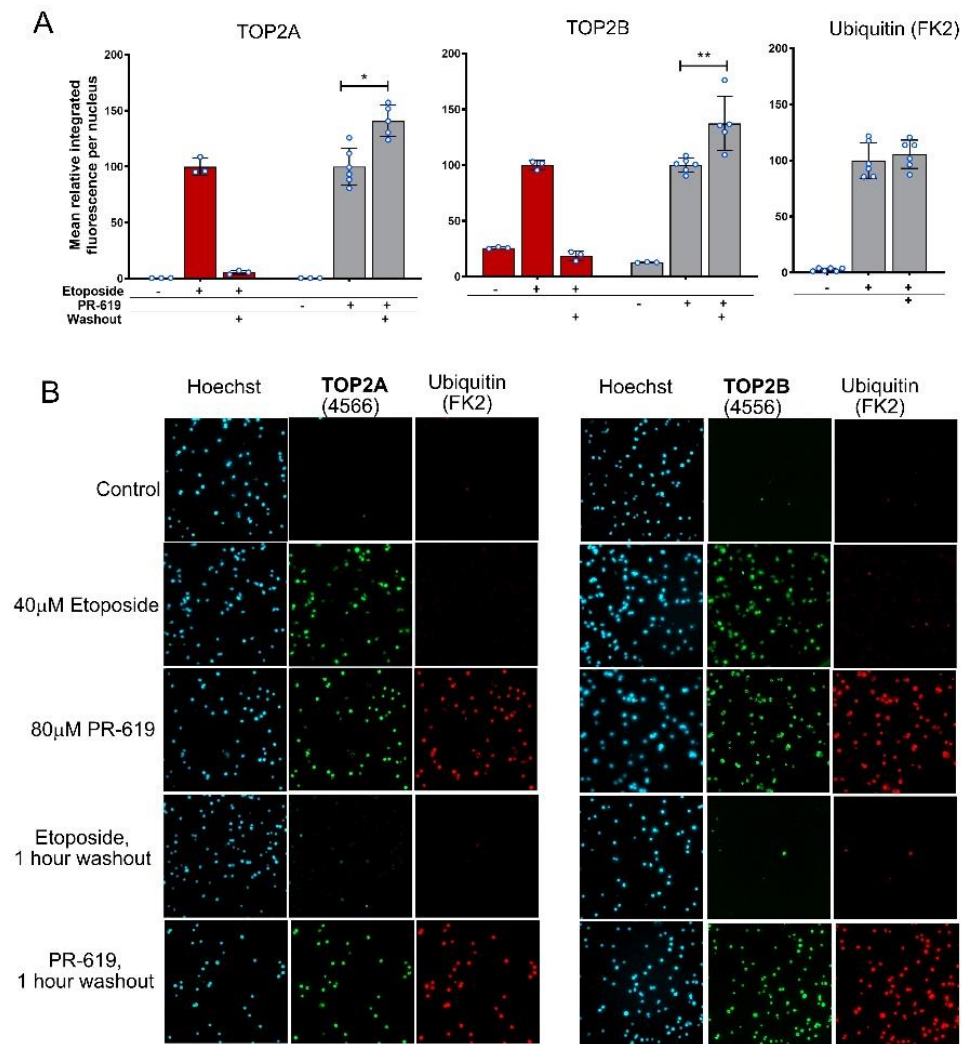Figure 7

Figure 8

Supplemental Data

The deubiquitinating enzyme inhibitor PR-619 is also a potent DNA topoisomerase II poison

Ian G. Cowell, Elise M Ling, Rebecca L. Swan, Matilda L. W. Brooks & Caroline A. Austin

Table of Contents

Supplementary Figure Legends

Supplemental Figure 1. The TARDIS assay lysis conditions remove chromatin proteins including histones and permit the specific detection of proteins covalently attached to genomic DNA. (A) TOP2A and histone proteins detected by immunofluorescent staining after standard paraformaldehyde immunofluorescent fixation (left) and TADIS extraction. Etoposide induces TOP2-DNA covalent complexes at least some of which are decorated with ubiquitin **(B)** and SUMO2/3 **(C).**

Supplemental Figure 2. PR-619 induces TOP2A and TOP2B DNA covalent complexes. K562 cells were incubated with PR-619 or etoposide at the concentrations indicated, or with solvent control (DMSO) for two hours. After washing in cold PBS cells were mixed with low melting point agarose at 37°C, spread on glass slides, lysed and extracted in situ. Covalent TOP2-DNA complexes and ubiquitinated proteins were detected and quantified by quantitative immunofluorescence using TOP2 isoform-specific TOP2 antibodies and anti-ubiquitin FK2. **(A & B)** Examples of images from slides used to quantify TOP2A (A), TOP2B (B) and ubiquitin (A & B) immunofluorescence. Bar=50μm. **(C)** Quantification of TOP2A, TOP2B and ubiquitin signal. Data are shown as scatter graphs showing median and interquartile ranges. Each spot represents the immunofluorescence signal from a single nucleus. Data shown are derived from a single representative experiment but are representative of three replicate experiments.

Supplemental Fig. 3 PR619 induces SUMOylated TOP2-DNA complexes. **(A)** K562 cells were treated with 50μM PR-619 with or without preincubation with the SAE inhibitor ML-792 (He *et al.*, 2017) (2μM, 4hr). Slides were prepared using the TARDIS protocol with TOP2A, TOP2B or anti-SUMO2/3 antibodies and were imaged using a 40X objective. **(B&C)** Cells were pre-treated with either ML-792(2μM, 4hr) or 2-DO8 (100μM, 18hr) before adding PR-619 (80μM) or etoposide (100μM) for two hours. TARDIS analysis was performed as in Supplemental Figs. 1&2. For (B) and (C), data are the mean of the median integrated fluorescence values per nucleus from three replicates +/- SD. Statistical analysis was performed by t-test

Supplemental Figure 4. Distribution of TOP2A in DRT-extracted HeLa cells. HeLa cells grown on glass coverslips were extracted in DRT buffer, fixed at room temperature with 4% paraformaldehyde in PBS and TOP2A was detected by immunofluorescence. Nuclei were counterstained with DAPI and images were recorded using 40X and 60X objectives. The contrast of the DAPI staining pattern was enhanced using a high pass filter (Photoshop) to visualize nucleoli which appear as low intensity regions within DAPI-stained nuclei.

Supplemental Figure 5. Distribution of TOP2B in DRT-extracted HeLa cells. HeLa cells grown on glass coverslips were extracted in DRT buffer, fixed at room temperature with 4% paraformaldehyde in PBS and TOP2B was detected by immunofluorescence. Nuclei were counterstained with DAPI and the contrast of the DAPI staining pattern was enhance using a high pass filter (Photoshop) to visualize nucleoli.
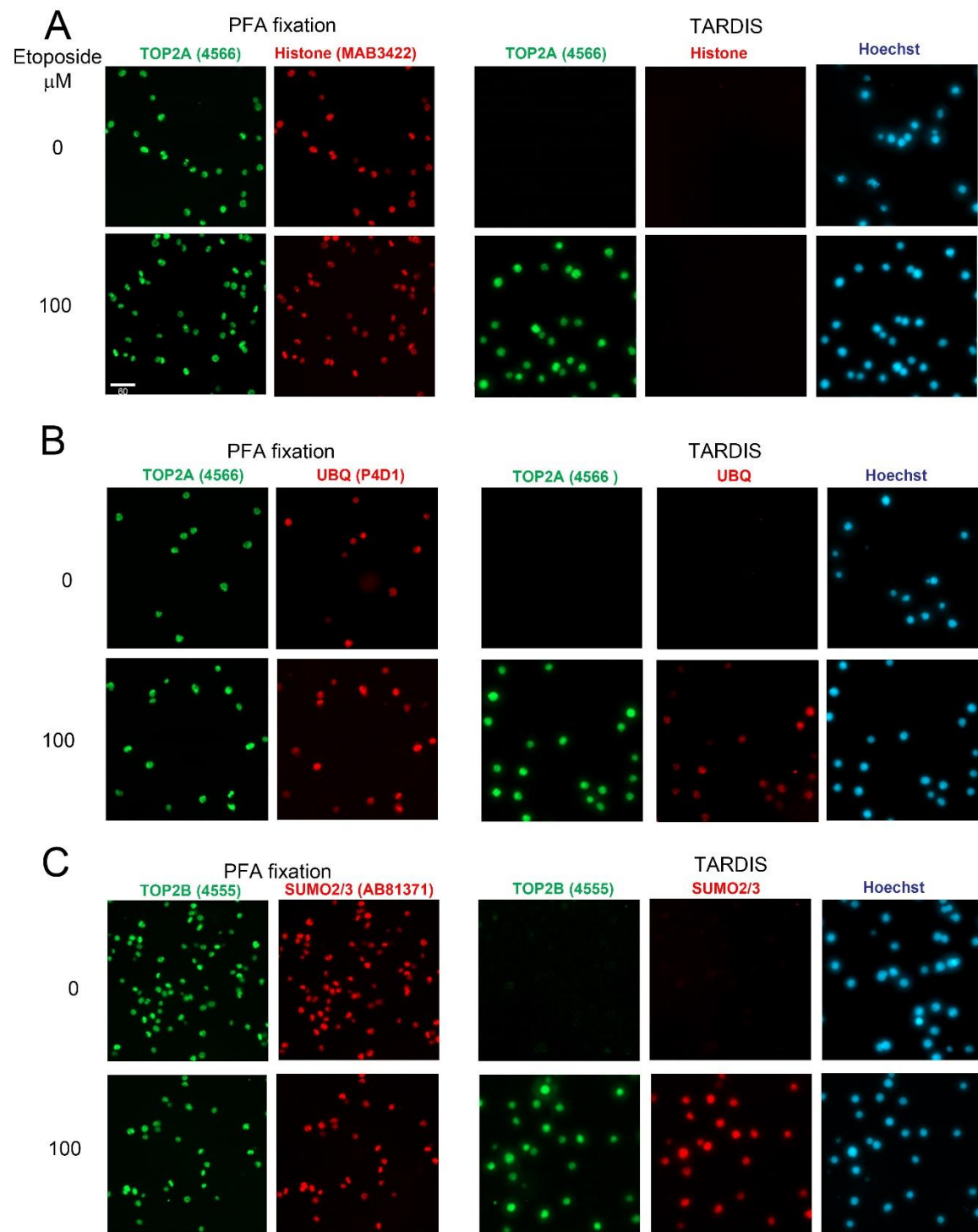
Supplemental Figure 6. Neither etoposide nor PR-619-induced covalent DNA complexes are affected by RNase treatment. K562 cells were treated with etoposide or PR-619 for two hours. Cells were embedded on agarose in glass slides and lysed and extracted in situ as described for the TARDIS assay. Slides were then incubated with DNAse-free RNase (50μg/ml) or PBS at 37°C before washing and detection of TOP2A or TOP2B by immunofluorescence. **(A)** TOP2A and TOP2B covalent-DNA complexes were quantified using the TARDIS assay. The results shown are the means of the median integrated fluorescence per nucleus from 4 separate fields of view from different regions of each slide. **(B)** Representative images captured using a 40X objective with a fixed exposure for each antibody.
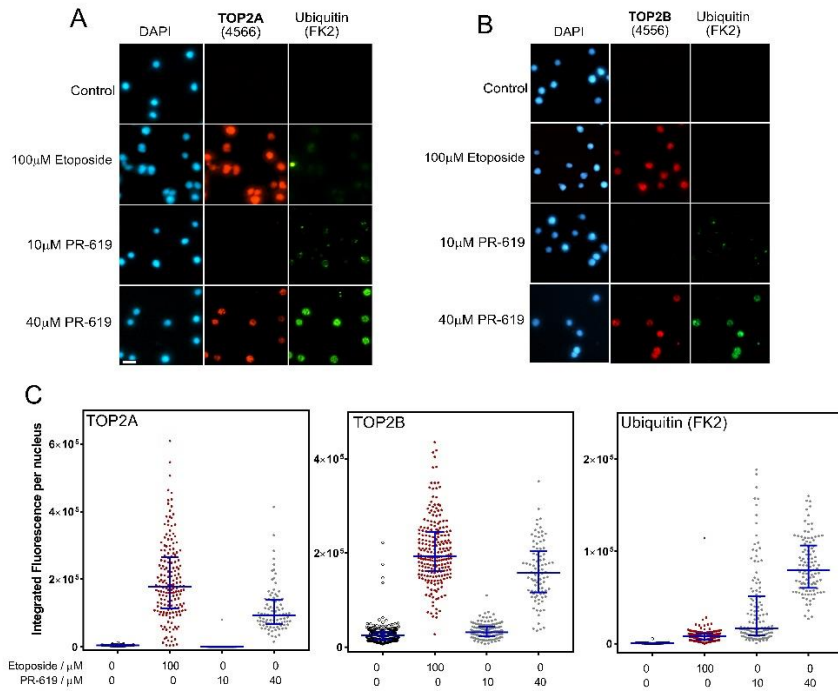
Supplemental Figure 7. Distribution of TOP2A-DNA complexes induced by etoposide, PR-619 or combinations of both drugs. K562 cells were treated with Etoposide or PR-619 individually for 150 minutes, with both for 150 min or with either one of the drugs first for 30 minutes before adding the other drug as indicated for 120 minutes and then collecting the cells for TOP2A TARDIS analysis. Images were acquired as z-stacks using a 40X objective, representative nuclei are shown from extended focus images.

Supplemental Figure 8 Distribution of TOP2B-DNA complexes induced by etoposide, PR-619 or combinations of both drugs. K562 cells were treated with Etoposide or PR-619 individually for 150 minutes, with both for 150 min or with either one of the drugs first for 30 minutes before adding the other drug as indicated for 120 minutes and then collecting the cells for TOP2B TARDIS analysis. Images were acquired as z-stacks using a 40X objective, representative nuclei are shown from extended focus images.

Supplemental Figure 9. Etoposide and PR-619 – induced H2AX phosphorylation. K562 cells were incubated with etoposide or PR-619 as indicated for 2hr and histone H2AX phosphorylation was determined by quantitative immunofluorescence. Inset, scatter graph representing data one replica experiment. Main figure means of medians derived from three replicate slides (individual values shown as circles).
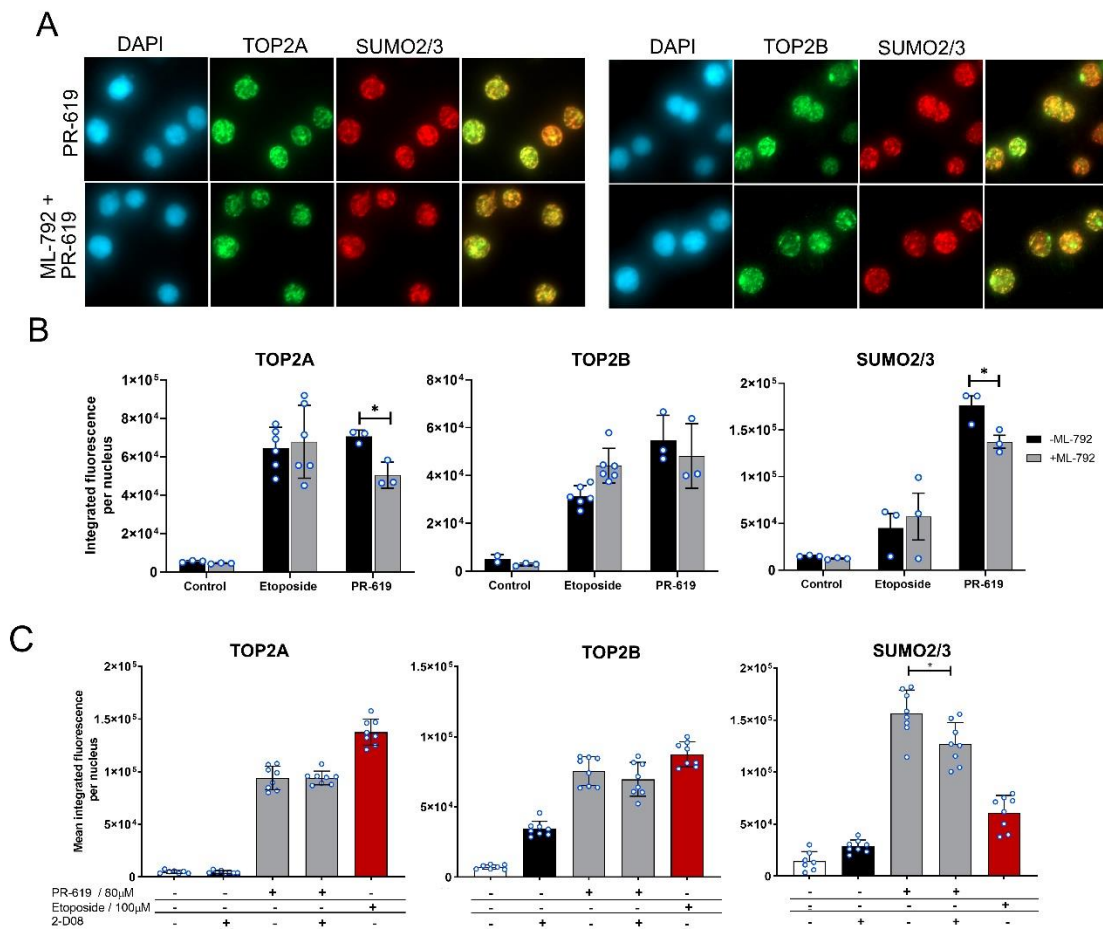
Supplemental Figures

A

PFA fixation   TARDIS

Etoposide µM

TOP2A (4566)   Histone (MAB3422)   TOP2A (4566)   Histone   Hoechst

0

100

B

PFA fixation   TARDIS

TOP2A (4566)   UBQ (P4D1)   TOP2A (4566)   UBQ   Hoechst

0

100

C

PFA fixation   TARDIS

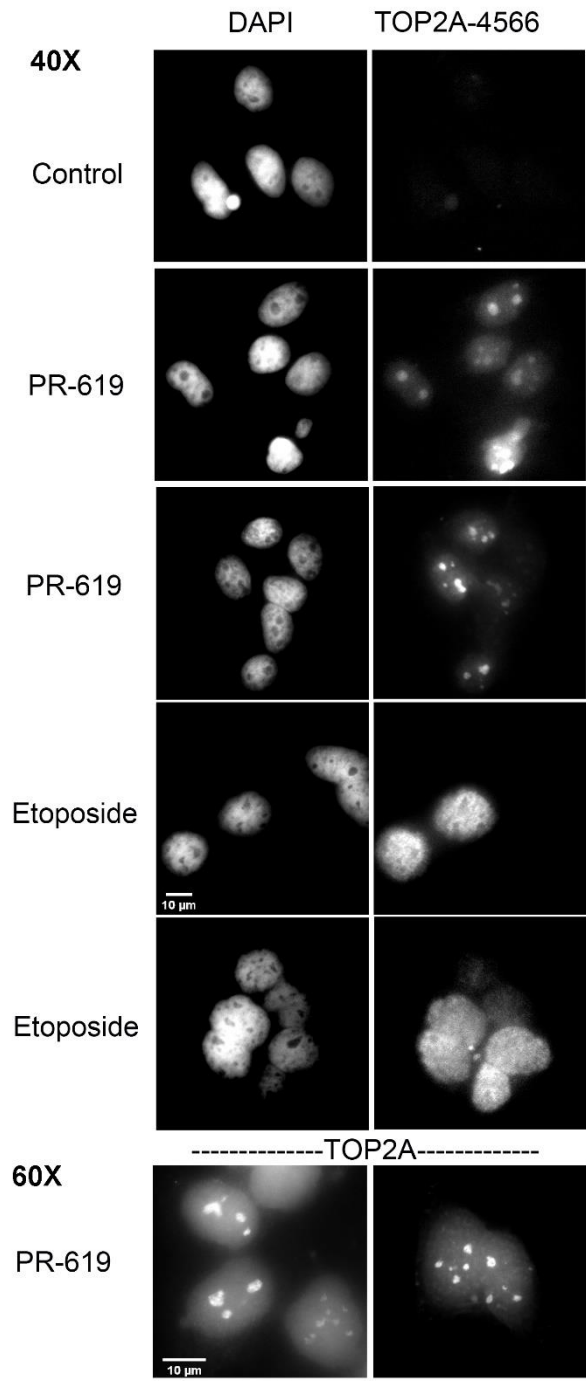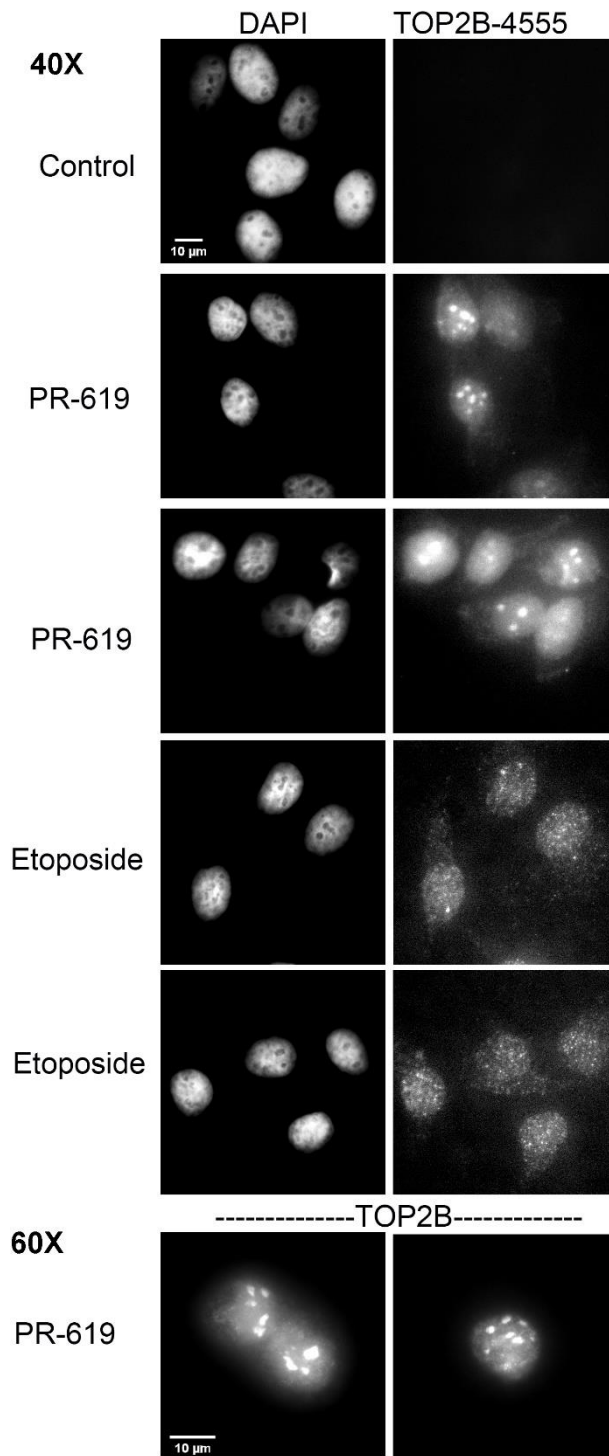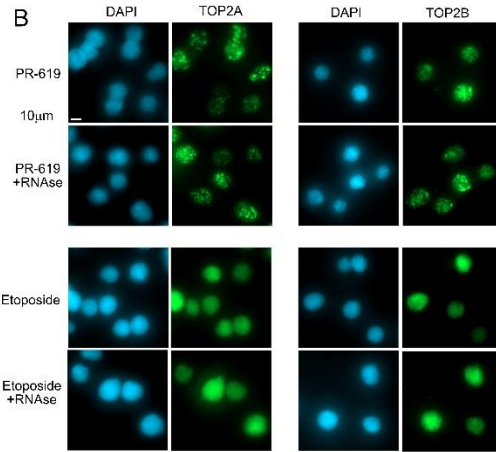TOP2B (4555)   SUMO2/3 (AB81371)   TOP2B (4555)   SUMO2/3   Hoechst

0

100

Supplemental Fig. 1
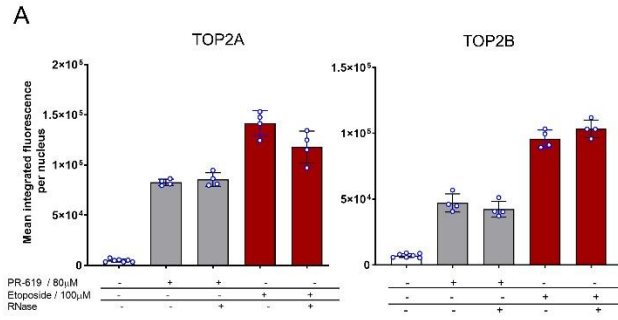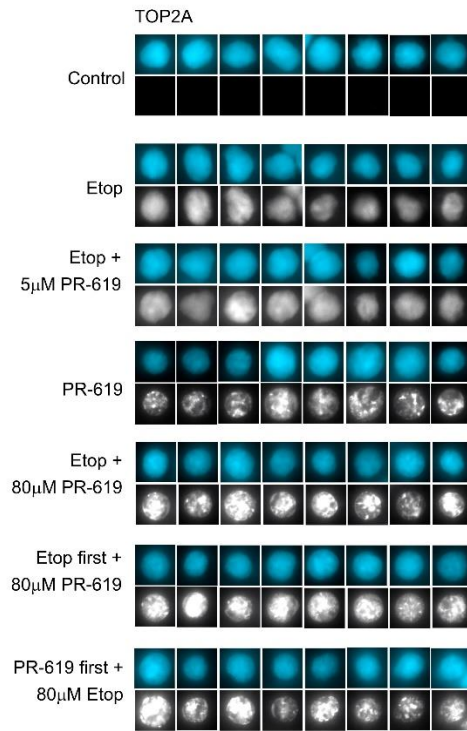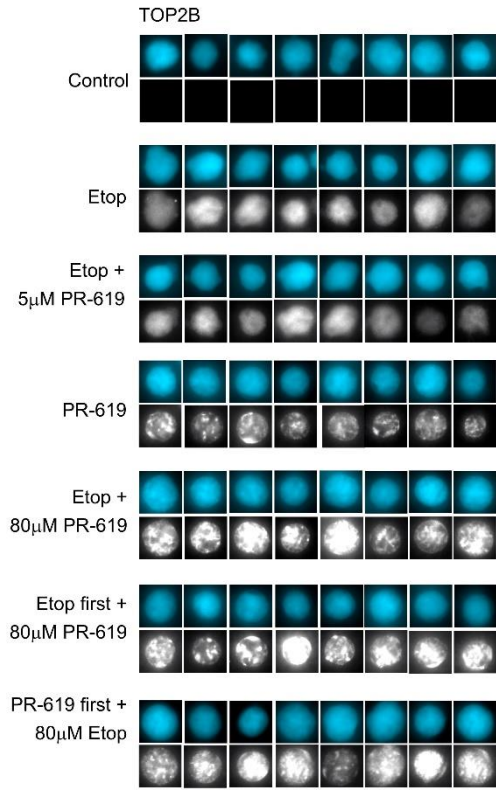
Supplemental Figure 2

Supplemental Figure 3

DAPI   TOP2A-4566

40X

Control

PR-619

PR-619

Etoposide

10 µm

Etoposide

--------------TOP2A-------------

60X

PR-619

10 µm

Supplemental Figure 4

Supplemental Figure 5

A

TOP2A

TOP2B

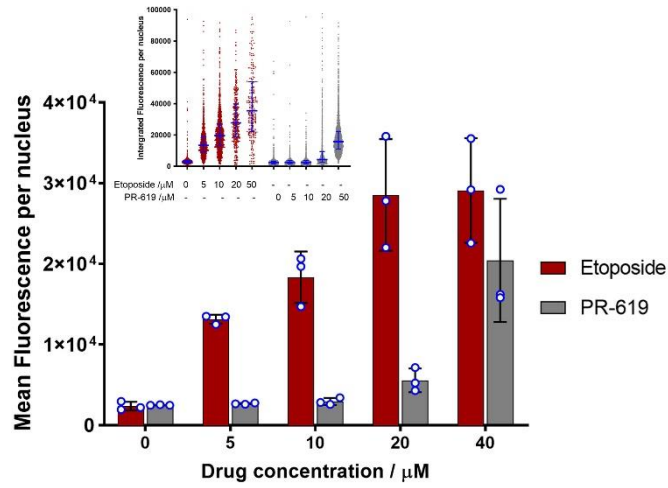| PR-619 / 80μM | - | + | + | - | - |
| Etoposide / 100μM | - | - | - | + | + |
| RNase | - | - | + | - | + |

B

Supplemental Figure 6

Supplemental Figure7

Supplemental Figure 8

Supplemental Figure 9